Received 6 June 2026; revised 15 July 2026; accepted 15 July 2026. Date of publication 20 July 2026; date of current version 31 July 2026.
The review of this article was arranged by Editor G. I. Ng.

Digital Object Identifier 10.1109/JEDS.2026.3714991

A Model for Hot-Electron Injection in the Passivation Layer of AlGaN/GaN HFETs Based on Monte Carlo Simulations

PIERPAOLO PALESTRI[1] (Senior Member, IEEE), LUCA SAYADI[2], ALESSANDRO RUGGIERI[1] (Graduate Student Member, IEEE), ANDREA MINETTO[3], GERHARD PRECHTL[2], LUCA SELMI[1] (Fellow, IEEE), AND OLIVER HÄBERLEN[2] (Senior Member, IEEE)

[1]Department of Engineering "Enzo Ferrari", University of Modena and Reggio Emilia, Modena 41125, Italy
[2]Infineon Technologies, Villach 9500, Austria
[3]Infineon Technologies Americas Corporation, El Segundo, CA 90245 USA

CORRESPONDING AUTHOR: P. PALESTRI (pierpaolo.palestri@unimore.it)

The work of Pierpaolo Palestri and Luca Selmi was supported in part by the NextGeneration EU, Italian Piano Nazionale di Ripresa e Resilienza (PNRR) M4C2 1.5, Ecosistema Territoriale di Innovazione dell'Emilia-Romagna (ECOSISTER) Spoke 3 Cascaded call Energy Efficient Embedded Electronics for PhotoVoltaics (E4PV) Project under Grant CUPE93C22001100001.

ABSTRACT We propose a lean model for hot-electrons in AlGaN/GaN HFETs, aimed at estimating the flux of carriers injected into the passivation layer above the AlGaN layer in the device drift region. Monte Carlo transport simulations are used to determine the hot-electron distribution and to verify the accuracy of the model equations. The model can be straightforwardly implemented into TCAD simulators to provide an estimate of the charge injected and/or trapped in the passivation during high drain voltage stress.

INDEX TERMS Gallium nitride simulation, Monte Carlo.

I. INTRODUCTION

Thanks to the wide bandgap and the reduced impact ionization rate compared to silicon, AlGaN/GaN Heterojunction Field-Effect Transistors (HFETs) can be operated at very high electric fields [1], allowing a shorter drift region to withstand the operating voltage. Combined with the high electron density and drift velocity of the 2D Gas (2DEG), AlGaN/GaN HFETs with superior performance can be fabricated for power switching and RF applications, ultimately resulting in higher energy efficiency and reduced size [2].

However, when GaN power HFETs operate in the saturation region, for instance during hard-switching in power converters, high fields and high currents are simultaneously present. The large energy gap and mean free path leads a fraction of electrons to gain a few electronvolts of kinetic energy. While being below the impact ionization threshold energy, ≈ 3.4 eV, this energy is large enough to bring hot-electrons out of the potential well at the heterointerface, to even cross the AlGaN, and to be injected in the passivation layer above [3], [4].

Typical passivation films contain plenty of deep levels with long emission time constants [5], and interface states where *hot*-electrons can be trapped. The build-up of negative trapped charge depletes the 2DEG, causing a detrimental dynamic-$R_{DS(on)}$ increase whose severity can range from a few percent to a complete pinch off of the 2DEG over the lifetime. Consequently, hot-carrier injection can limit the drift region scaling to lengths well above the minimum posed by the onset of impact ionization, thus hindering full exploitation of GaN's potential.

Physically accurate hot-electron modeling in GaN HFETs can provide important insights to support the development of GaN power HFET technology [6], [7], [8], [9]. At present, however, GaN HFETs design mainly relies on drift-diffusion or hydrodynamic transport models [8], [10], [11], [12], [13] implemented in commercial TCAD simulators, which are inherently not well suited to study high energy carriers [14].

For instance, the lucky-electron [15], [16] and the Fiegna models [17], developed to extend drift-diffusion transport to hot-carrier injection in silicon devices, assume energy distributions that are unrealistic for GaN transistors (as shown in this work). Using these models for GaN HFETs is also unjustified because they do not account for the AlGaN layer between the GaN channel and the passivation. Monte Carlo (MC) transport simulations can predict the hot-carriers' energy distribution accurately [18], and analysis of bulk GaN material and GaN HFETs with the MC solution of the Boltzmann Transport Equation have been presented in [19], [20], [21], [22], and [23]. However, they are too time-consuming for systematic use to engineer device architectures; in fact, we are not aware of studies focusing, e.g., on hot-electron injection in the passivation layer of AlGaN/GaN HFETs.

To fill this important gap for GaN technology development, this paper presents: *i*) an analysis of hot-electron transport in AlGaN/GaN HFETs based on the statistical solution of the BTE by MC methods, *ii*) a novel simple model (calibrated on the MC results) for the hot-electron flux across a passivation/AlGaN/GaN stack, amenable to implementation in TCAD via, e.g., Physical Model Interface scripts [24]. Our approach effectively combines simulations of vertical transport and the conduction band discontinuities, with lateral transport in a uniform electric field representative of the drift region. When combined with appropriate trapping/detrapping models, the results could provide accurate simulations of dynamic-$R_{DS(on)}$ under relevant bias conditions for state of the art GaN HFETs.

The paper is organized as follows. The MC procedure is described in Sect. II. The proposed semi-analytical model is detailed in Sect. III. Conclusions and future perspectives are given in Sect. IV.

II. MONTE CARLO TRANSPORT MODEL

A. BAND STRUCTURES AND SCATTERING MECHANISMS

Accurate knowledge of the electron energy distribution in the GaN channel and in the AlGaN barrier is key to quantitatively evaluating the flux and the current density of hot-electrons injection in the passivation layer. To this end, we have developed a single-particle solver of the BTE in GaN and AlGaN using the MC method [25]. Since we focus on hot-carrier effects involving high-energy electrons in the conduction band, Pauli's exclusion principle can be safely ignored, as motivated in [25]. Consequently, the carrier distributions can be normalized to any carrier concentration.

The conduction band model for GaN consists of analytical, spherical, and non-parabolic Γ_1, Γ_3, and U valleys. Due to the low scattering rate in the Γ_1 valley, at high drain bias electrons have a high probability to gain enough energy to scatter into the Γ_3 and U valleys ($\approx$ 2 eV). Once the satellite valleys become accessible, the sudden increase in the density of final states boosts inter-valley non-polar optical phonon scattering, and further electron heating becomes much less probable.

The scattering mechanisms for GaN include optical polar, non-polar phonon, and acoustic (elastic) phonon scattering. In the absence of clear indications whether (for analytical bands) non-polar optical phonon scattering should be included as an intra-valley mechanism in the Γ_1 valley, or only as an inter-valley one, we have followed [22] and implemented them also as intra-valley scattering. Ionized impurity and piezoelectric scattering have also been implemented. Their impact on the electron energy distribution is negligible within the range of electric field values considered here. They have a remarkable impact on the low-field mobility, whose faithful description, however, is not critical for the goals of this work.

As for the AlGaN layer, we assume a typical Al molar fraction value of 20%, and the band structure parameters (effective masses and valley offsets) are linearly interpolated between those of GaN and AlGaN. The conduction band minimum is shifted upward by $\Delta E_C \approx 0.26$ eV. The scattering mechanisms are the same of GaN but alloy scattering is also included.

The dispersion relation of the passivation material, which is necessary to properly compute the injected flux according to energy and momentum conservation, is also non-parabolic. For simplicity, if not otherwise stated, we assume the same dispersion relation parameters as for GaN, except that the bottom of the conduction band forms an energy discontinuity E_{b0} with respect to the AlGaN one. The impact of the electron effective mass in the passivation is analyzed in Subsect. III-E.

The model parameters used in this work, reported in Table 1, are consistent with those of other Monte Carlo simulators for GaN reported in the literature.

B. BENCHMARK AGAINST LITERATURE RESULTS

We briefly benchmark our Monte Carlo BTE solver against literature results for the average velocity and average energy of bulk GaN as a function of electric field. Fig. 1 shows that our simulator is in agreement with most of the other literature works listed in Table I. The large spread of the curves is partly explained by noting that [26] considers a much lower separation between Γ_1 and U valleys compared to other authors. This influences the velocity at high lateral field, that decreases as the energy offset between the Γ_1 and U valley decreases. On the other hand, [22] considers a much larger non parabolicity of the Γ_1 valley, leading to lower group velocity at high energy and higher scattering rates, while [21] has a much higher coupling factor for non-polar phonons compared with other authors.

In addition to the previous analysis, we have verified that the same velocity- and energy-field curves of the other published work are obtained if we use in our Monte Carlo transport model the same parameter sets reported by the respective authors (not shown).

Fig. 2 compares the electron energy distributions obtained with our analytical bands Monte Carlo transport simulator to those of full-band simulations [21], confirming the appropriateness of the analytical band description for our hot-electron problem.

TABLE 1. Band structure and scattering parameters of the monte carlo simulator.

Symbol	Description	This work	[20]	[19]	[26]	[22]	[27]	[21]	[23]	Units
ε_0	low freq. permittivity	8.9	9.5	8.9	8.9	8.9	8.9	9.5	9.7	ε_0
ε_∞	high freq. permittivity	5.35	5.35	5.35	5.35	5.35	5.35	5.35	5.28	ε_0
ω_{ph}	opt. ph. energy	91	92	93	92	91	92	92	91	[meV]
D_{op}	coupl. optical ph.	$3 \cdot 10^{11}$	$1 \cdot 10^{11}$	$1 \cdot 10^{11}$	n.a.	$3.8 \cdot 10^{10}$	$1 \cdot 10^{11}$	$4 \cdot 10^{11}$	$1 \cdot 10^{11}$	[eV/m]
D_{ac}	coupl. acoustic ph.	8.3	8.3	8.3	8.3	4.0	8.3	8.3	8.3	[eV]
$m_{\Gamma 1}$	eff. mass. $\Gamma 1$ valley	0.2	0.2	0.2	0.2	0.2	0.21	0.2	0.2	$[m_0]$
$\alpha_{\Gamma 1}$	non parab. $\Gamma 1$ valley	0.2	0.19	0.183	n.a.	0.58	0.189	0.2	0.37	$[eV^{-1}]$
$m_{\Gamma 3}$	eff. mass. $\Gamma 3$ valley	0.28	0.4	0.6	n.a.	0.28	0.4	0.5	0.3858	$[m_0]$
$\alpha_{\Gamma 3}$	non parab. $\Gamma 3$ valley	0.2	0.0	0.029	n.a.	0.0	0.029	0.22	0.22	$[eV^{-1}]$
$\Delta E_{\Gamma 3}$	energy offset $\Gamma 3$ valley	2.2	1.75	2.1	n.a.	2.23	2.2	2.4	2.2717	[eV]
m_U	eff. mass. U valleys	0.33	0.24	0.4	1.0	0.33	0.25	0.5	0.2856	$[m_0]$
α_U	non parab. U valleys	0.2	0.17	0.065	n.a.	0.0	0.065	0.385	0.385	$[eV^{-1}]$
ΔE_U	energy offset U valleys	2.0	1.49	2.0	1.2	1.95	1.9	2.0	2.4	[eV]

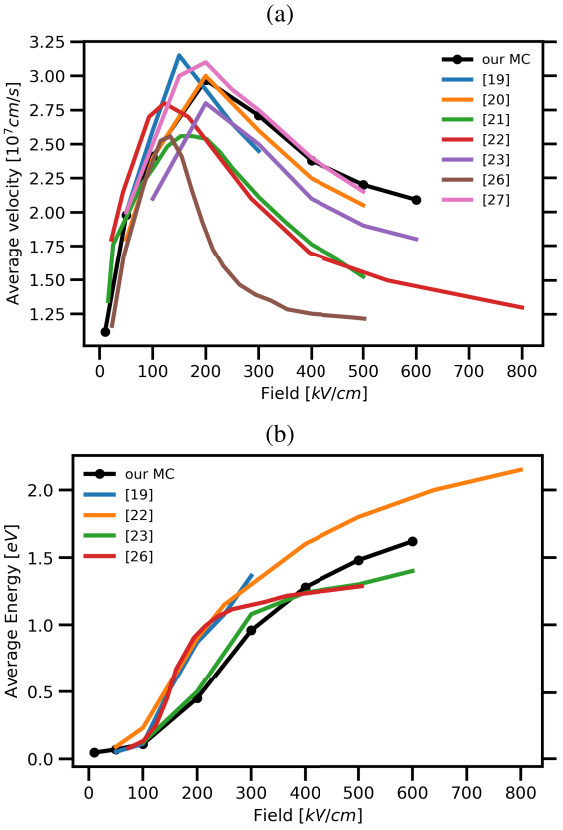

FIGURE 1. (a) Simulated average electron velocity and (b) average electron energy as a function of the electric field in bulk GaN, compared with results from other Monte Carlo BTE solvers in the literature [19], [20], [21], [22], [23], [26], [27], see Tab. 1.

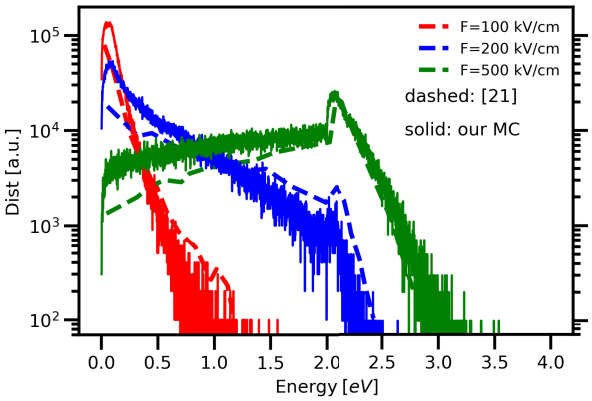

FIGURE 2. Simulated energy distributions in bulk GaN for different values of the electric field *F*, compared against the Full-Band Monte Carlo results from [21].

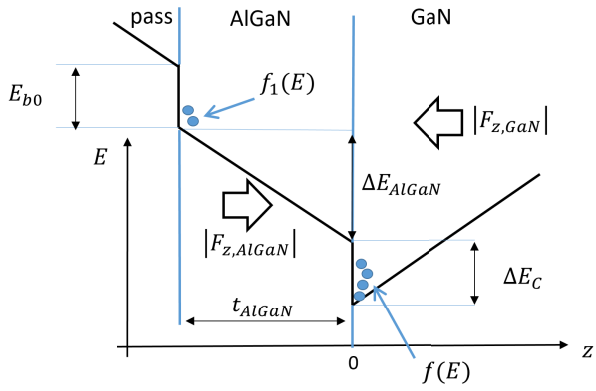

FIGURE 3. Sketch of the band diagram of the AlGaN/GaN stack considered in this work.

C. SIMULATION DOMAIN AND SIMULATION PROCEDURE

The simulation domain, depicted in Fig. 3 [25], consists (in the vertical direction, z) of a semi-infinite AlGaN/GaN hetero-structure and a passivation layer. Due to the polarization sheet charge at the hetero-junction, the vertical component of the electric field (F_z) points in opposite directions in the AlGaN and GaN layers, henceforth confining the low kinetic energy electrons at the hetero-interface. We assume that F_z is uniform in the GaN and AlGaN regions (with different values $F_{z,GaN}$ and $F_{z,AlGaN}$, respectively), which is a reasonable idealization for a HFET biased in the semi-ON state. Indeed, in this case, the electron density in the essentially undoped depletion region is small, and its impact on F_z can be neglected.

Having in mind the goal of developing a compact analytical model for hot-carrier injection, we assume that the electron energy distribution in each vertical slice of the drift region is at equilibrium with the local lateral electric field component F_x and we set the same F_x value in GaN and

AlGaN, in accordance with Gauss's law at the interface. Then, we simulate a single slice of the drift region at a given lateral field F_x. As a result, F_x, $F_{z,GaN}$ and $F_{z,AlGaN}$, as well as E_{b0}, become parameters of the model in the following.

The simulation proceeds as follows. Electrons are injected one by one in the GaN channel, where they gain kinetic energy while drifting under the action of F_x and until convergence of the statistical estimators of interest is reached (notably, the flux of hot-carriers injected into the passivation). The vertical field in the GaN pushes the electrons toward the heterointerface. When they hit the interface, they are transferred to the AlGaN only if conservation of energy and parallel momentum is possible, also considering the ΔE_C; otherwise, they are reflected back into the GaN. Once transferred in the AlGaN, electrons are pushed back into the GaN by the opposite F_z. However, those *lucky* electrons that have enough energy to diffuse against the field can move up to the AlGaN/passivation interface. Here, the above conservation laws are applied again (taking into account the E_{b0} barrier), and if they are satisfied, the event is recorded, and the data is used to calculate the rate of hot-electron injection into the passivation (r).

The MC transport procedure provides statistical estimates of the following quantities: *i*) the probability density function for the electron position, $P(z)$, in cm^{-1}; *ii*) the occupation function (i.e. the electron energy distribution divided by the DoS) of the electrons at the AlGaN/GaN interface, $f(E)$; *iii*) the average frequency at which electrons are injected into the passivation, r in s^{-1}. Since all quantities are, by construction, independent of x, the ratio $r/P(z=0^+)$ in cm/s, is equal to the ratio between the electron flux across the AlGaN/passivation interface, Φ in $\mathrm{cm}^{-2}\mathrm{s}^{-1}$ and the electron concentration on the GaN side of the AlGaN/GaN interface, n_{ITF} in cm^{-3}. As shown in [25], Φ/n_{ITF} is independent of $F_{z,GaN}$, reason why we have chosen this ratio to build our semi-analytical model in Sect. III. The approach is analogous to the one embraced in Fiegna's model [17], where the hot-electron flux at the target interface (AlGaN/passivation in our case) is proportional to the carrier concentration at the starting interface (AlGaN/GaN in our case). This is legitimate since we are solving the linear BTE (no Pauli's exclusion principle) and we focus on the hot-carriers.

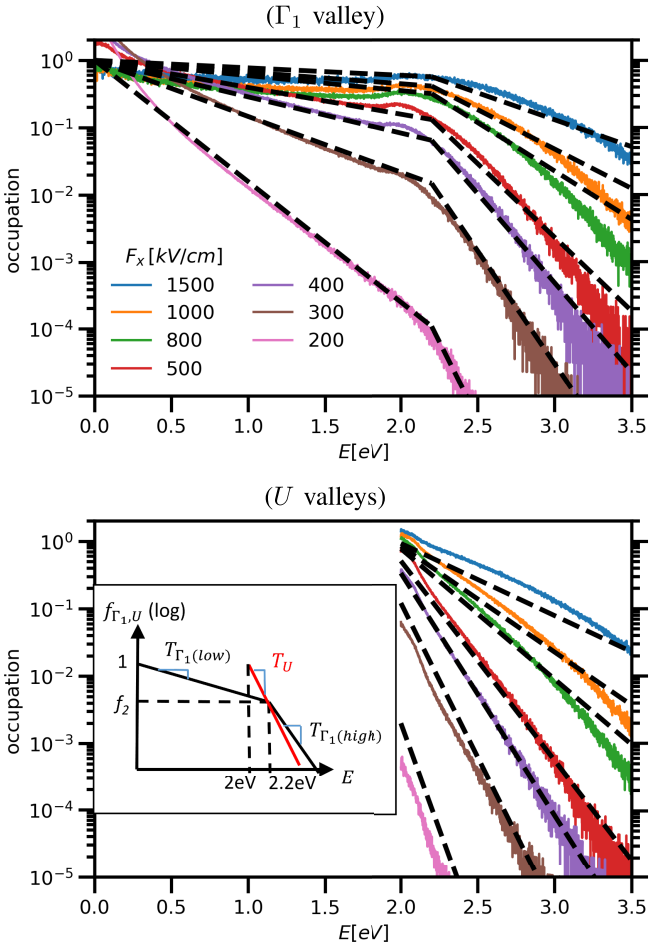

FIGURE 4. Occupation function (i.e. energy distribution divided by the density of states) for Γ_1 (top) and U (bottom) valleys for different values of the lateral electric field F_x. The distributions are collected at the top of the GaN layer, within 1 nm from the interface with AlGaN, and normalized in such a way that the Maxwellian fits (dashed lines, effective temperatures given by (1)-(2)) start from one at zero energy. The same normalization factor is used for Γ_1 and U distributions. The inset of the bottom panel defines the main features of the analytical occupation functions.

III. SEMI-ANALYTICAL MODEL

A. OCCUPATION FUNCTIONS AT THE GAN/ALGAN INTERFACE

As already stated in Sect. II, the key element of hot-electron injection models is the energy occupation function in the GaN channel and at AlGaN/passivation interface. Reference [15] assumes heated Maxwellians, whereas in [17], an analytical expression obtained from an approximate solution of the BTE is used. Unfortunately, neither of the two analytical expressions is applicable to GaN as discussed below. Fig. 4 reports sample occupation functions at $z = 0$ for the Γ_1 and U valleys for different lateral effective fields. We verified that these normalized occupations have a negligibly weak dependence on $F_{z,GaN}$, $F_{z,AlGaN}$ and t_{AlGaN}. This important finding greatly simplifies the development of the analytical model, since only the F_x dependence has to be modeled.

We observe in Fig. 4, top graph, that the occupation function of the Γ_1 valley is well approximated by a piecewise Maxwellian function, with different effective temperatures above and below $\approx$ 2 eV, which is close to the U valleys minimum. In the U valleys, the distribution is simply Maxwellian, but with a different effective temperature than in the Γ_1 valley. Although included in the MC simulator, the Γ_3 valley has not been included in the model since its carrier density is negligible compared to the other valleys. The heated Maxwellian shape is mostly due to *non-polar* optical phonon scattering in the Γ_1 valley, and frequent transfer of electrons between GaN and AlGaN (where *alloy* scattering

is very intense) which effectively randomizes the momentum and rethermalizes the carriers.

We can therefore represent the occupation function of the dominant Γ_1 and U valleys as sketched in the inset of Fig. 4, where the knee of the Γ_1 energy distribution is set 2.2 eV above the Γ_1 minimum; hence slightly above the U valley minimum. The Γ_1 and U valleys distributions cross each other at approximately this energy, which underlines the importance of intra-valley scattering. The effective temperature of the heated Maxwellians is well described as a function of the lateral field by the following linear interpolation formulae:

$$0 < E < 2.2\text{eV}\ \ T_{\Gamma_1(low)} = 2800 + 32.5 \cdot (|F_x| - 200) \quad (1)$$

$$E > 2.2\text{eV}\ \ T_{\Gamma_1(high)} = 1100 + 4.0 \cdot (|F_x| - 200) \quad (2)$$

$$E > 2.0\text{eV}\ \ T_U = 800 + 3.0 \cdot (|F_x| - 200) \quad (3)$$

where F_x is expressed in kV/cm and the temperatures are in K. Indeed, the dashed lines in Fig. 4 are obtained with the formulae above. Despite their simplicity and some loss of accuracy above 3 eV, Eqs. (1)-(3) provide a satisfactory estimation of the hot-electron injection flux, as discussed in the following paragraphs.

B. EFFECTIVE BARRIER FOR INJECTION

To derive an analytical expression for the electron flux entering the passivation, Φ, from the analytical occupation functions in GaN, we start with the heuristic argument that if the hot-carrier trajectories were purely vertical, then electrons leaving the 2DEG would cross the AlGaN layer and reach the passivation if they could overcome the energy barrier due to the sum of ΔE_C (≈ 0.26 eV for 20% Al fraction), and the $\Delta E_{AlGaN} = q\,|F_{z,AlGaN}|\,t_{z,AlGaN}$ generated by the repulsive vertical field in the AlGaN. However, while traveling across the AlGaN layer, electrons convert the potential energy associated with the lateral field into kinetic energy, which is partly redistributed in the vertical direction through isotropic scattering (e.g. alloy scattering). This mechanism increases the carrier's perpendicular energy, which can be interpreted as an effective barrier lowering proportional to $|F_x| \cdot t_{z,AlGaN}$ via an empirical coefficient η. We thus define an *effective barrier*:

$$E_{b1} = \Delta E_C + q|F_{z,AlGaN}| \cdot t_{AlGaN} - q\eta\,|F_x| \cdot t_{AlGaN}. \quad (4)$$

To illustrate the effects of barrier lowering, Fig. 5 shows the normalized flux Φ/n_{ITF} from MC simulations versus the total energy barrier in two relevant cases. The blue curve refers to a hypothetical device without AlGaN layer (hence, $\Delta E_C = 0$) where channel hot-electrons are injected directly into the passivation, and the barrier E_{b0} is artificially varied. This curve probes how much the flux would change in the absence of heating by F_x and backscattering in the AlGaN. We see that the injection efficiency reduces very fast as the barrier is increased above $\approx 2eV$, that is consistent with the shape of the occupation functions in Fig. 4 (e.g. orange curve). The solid red curve, instead, is obtained changing ΔE_{AlGaN} by increasing t_{AlGaN} and setting $E_{b0} = 0$. The

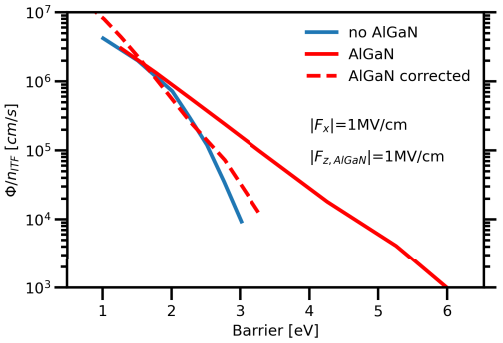

FIGURE 5. Flux injected into the passivation, Φ, normalized to the interface concentration in the GaN, n_{ITF}. Blue line: passivation/GaN stack, without AlGaN; the barrier on the x-axis is equal to E_{b0}. Red lines: passivation/AlGaN/GaN stack, where t_{AlGaN} is varied. Red solid line: the barrier on the x-axis (E_{b1}) is computed for $\eta = 0$ (no barrier lowering term in (4)). Red dashed line: the barrier on the x-axis E_{b1} is computed with (4), $\eta \approx 0.5$. The flux for the dashed red line is multiplied by $1/\eta_{BS}$ with $\lambda = 3$nm.

different slopes of the red and blue solid curves, and the crossing for a barrier of $\approx 2eV$, point out that for the same total vertical energy barrier the AlGaN layer affects the injection by: (i) reducing the flux due to back-scattering, as seen at low barriers; (ii) reducing the slope of the Φ/n_{ITF} vs barrier curve, and thus increasing injection in the passivation at large barrier values.

The dashed red curve in Fig. 5 is the same case as the solid red line, but adding the barrier lowering term in (4) for the x-axis and rescaling the flux provided by the MC by the factor

$$\eta_{BS} = \frac{\lambda}{\lambda + t_{AlGaN}} \quad (5)$$

that, according to quasi-ballistic transport theory [28], is the probability to survive backscattering in the AlGaN layer. Counting the average number of simulated scattering events in the AlGaN layer over a wide number of cases, and comparing the distribution at the AlGaN/passivation interface with that at the AlGaN/GaN one, we extracted a carrier mean free path $\lambda = 3$ nm and $\eta = 0.5$. After this correction, the red-dashed curve closely matches the blue line. This means that the computation of the injected flux in case of interest, with a gradual barrier in the AlGaN, can be simplified by leading it back to the crossing of a single effective barrier.

C. INJECTED FLUX

Monte Carlo simulations show that the contribution of the U and Γ_3 valleys to the hot-carrier flux injected into the passivation is always below 5% over a wide range of electric field configurations; therefore, for the sake of a lean, efficient model, these valleys are neglected in the calculation of Φ, and we focus on the Γ_1 valley only. Following the previous reasoning about back-scattering and effective barrier, the results of MC simulations suggest that the main effect of the AlGaN is to back-scatter some of the hot-electrons and to filter out those at energy below the effective barrier E_{b1}. We thus write energy occupation function in the AlGaN at

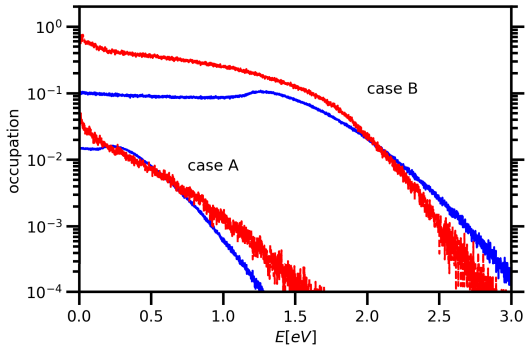

FIGURE 6. Occupation function (i.e., carrier energy distribution divided by the density of states) for the Γ_1 valley at the AlGaN/passivation interface (red curves) compared with the one at the GaN/AlGaN interface divided by η_{BS} and shifted by E_{b1} (blue curves) Case A: $|F_x| = 500kV/cm$, $t_{AlGaN} = 20nm$, $\Delta E_{AlGaN} = 2$ eV. Case B: $|F_x| = 1000kV/cm$, $t_{AlGaN} = 10nm$, $\Delta E_{AlGaN} = 1$ eV. In both cases, $|F_{z,GaN}| = 0.5MV/cm$ and $|F_{z,AlGaN}| = 1.0MV/cm$. The energy reference is the bottom of the conduction band at the AlGaN side of the AlGaN/passivation interface.

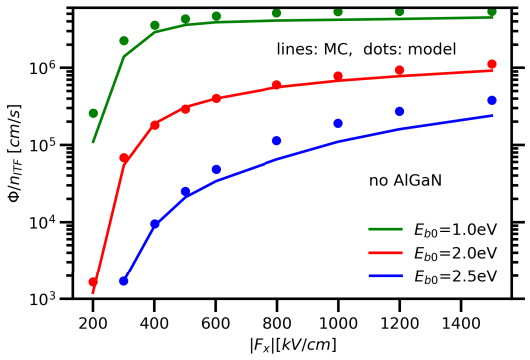

FIGURE 7. Flux Φ into the passivation normalized to the interface concentration n_{ITF} as a function of the lateral field for different values of E_{b0} in a passivation/GaN structure without AlGaN layer. Dots: MC simulations; solid lines: analytical model.

the interface with the passivation as:

$$f_{1,\Gamma_1}(E) = \eta_{BS} \cdot f_{\Gamma_1}(E + E_{b1}), \tag{6}$$

where $f_{\Gamma_1}(E)$ and $f_{1,\Gamma_1}(E)$ are the distribution function at the GaN and AlGaN side of the GaN/AlGaN and AlGaN/passivation interfaces, respectively, while E refers to the bottom of the conduction band at the same location. Direct comparison between electron distributions at the AlGaN/passivation interface and those at the GaN/AlGaN adjusted following (6), i.e., divided by η_{BS} and shifted by E_{b1}, is provided for two cases in Fig. 6. A good agreement is found between the two in the relevant energy ranges.

Assuming that the momentum distribution is isotropic, as suggested by the large scattering rate at high energy, it is now straightforward to calculate the flux Φ of electrons overcoming the passivation barrier E_{b0} by the same arguments used for thermionic emission at heterojunctions. The flux above the barrier between AlGaN and passivation is computed as

$$\Phi = \frac{2}{(2\pi)^3} \int v_\perp(\mathbf{k}) f_{1,\Gamma_1}(E(\mathbf{k})) d^3\mathbf{k}, \tag{7}$$

where $v_\perp = (1/\hbar)\partial E/\partial k_\perp$ is the electron velocity perpendicular to the interface, and $\hbar$ is the reduced Planck's constant. Assuming conservation of energy and parallel momentum and transforming the integral in k-space into an integral in energy one finds

$$\Phi = \frac{\eta_{BS} A}{q k_B^2} \int_{E_{b0}}^{\infty} \Theta(E) f_{\Gamma_1}(E + E_{b1}) dE, \tag{8}$$

where the lowest integration energy filters electrons above the AlGaN/passivation barrier, $A = 4\pi q m_{\Gamma_1} k_B^2/h^3$ is Richardson's constant, k_B and h are Boltzmann's and Planck's constant respectively, and

$$\Theta(E) = \min\left\{ E\left(1 + \alpha_{\Gamma_1} E\right), \right.$$
$$\left. \frac{m_{pass}}{m_{\Gamma 1}}(E - E_{b0})\left[1 + \alpha_{pass}(E - E_{b0})\right] \right\} \tag{9}$$

accounts for the finite density of states at the two sides of the junction. Note that if $m_{pass} = m_{\Gamma_1}$, $\alpha_{pass} = 0$, and the distribution function is Maxwellian, then Equation 8 reduces to the usual formula for thermionic emission [29]. Equation 8 can be numerically integrated using the analytical expressions (1)- (3) for the occupation function.

To reduce the number of model parameters, in the following we will set m_{pass} and α_{pass} to the same values as the Γ_1 valley of GaN, if not otherwise stated. The effect of m_{pass} is scrutinized in Subsect. III-E.

The injected flux, equation (8), is then normalized by the electron concentration in the GaN at the interface with AlGaN, n_{ITF}, obtained by integrating the product between the occupation functions and the density of states, D_ν of the Γ_1 and U valleys:

$$n_{ITF} = n_{\Gamma_1(low)} + n_{\Gamma_1(high)} + n_U, \tag{10}$$

where

$$n_{\Gamma_1(low)} = \int_0^{2.2\,eV} D_{\Gamma_1}(E) f_{\Gamma_1}(E) dE$$
$$n_{\Gamma_1(high)} = \int_{2.2\,eV}^{\infty} D_{\Gamma_1}(E) f_{\Gamma_1}(E) dE$$
$$n_U = \int_{\Delta E_U}^{\infty} D_U(E - \Delta E_U) f_U(E) dE$$
$$D_\nu = \frac{g_\nu (2m_\nu)^{3/2}}{2\pi^2\hbar^3} \sqrt{E(1 + \alpha_\nu E)}(1 + 2\alpha_\nu E), \tag{11}$$

$\nu = \Gamma_1, U$ is the valley index, g_ν is the number of equivalent minima (1 for Γ_1, 6 for the U valleys), and the $f_\nu(E)$ are piece-wise Maxwellians with temperatures given in (1)-(3). Here, the U valley is included due to its non-negligible contribution to the population of cold carriers entering the n_{ITF}.

D. MODEL VERIFICATION

Fig. 7 compares the analytical model with MC simulations of a structure without AlGaN layer, that is $\eta_{BS} = 1$ in (8), $\Delta E_C = 0$, and $\Delta E_{AlGaN} = 0$. The good agreement confirms the

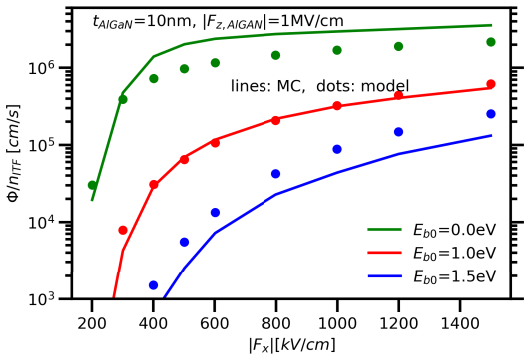

FIGURE 8. **Flux Φ into the passivation normalized to the concentration n_{ITF} in the GaN at the interface with AlGaN for a structure with 10 nm AlGaN, $|F_{z,AlGaN}| = 1$ MV/cm, for different values of E_{b0}. Dots: MC simulations, solid lines: analytical model.**

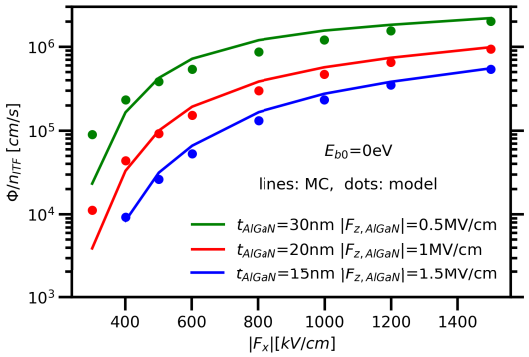

FIGURE 9. **Flux into the passivation normalized to the concentration in the GaN at the interface with AlGaN for structures with different AlGaN thicknesses and vertical fields (different E_{b1}), with $E_{b0} = 0$ eV. Dots: MC simulations, solid lines: analytical model.**

validity of equations (1) - (3) and the assumption of isotropic momentum distribution underlying equation (8).

Fig. 8 compares the analytical model with MC simulations of a device with AlGaN layer. The barrier E_{b0} is varied for fixed AlGaN thickness and vertical field.

Conversely, Fig. 9 shows Φ/n_{ITF} for $E_{b0} = 0$ eV and varying AlGaN thickness and vertical field.

The last two figures show that the semi-analytical model reproduces well the MC results using the calibrated values of the only two available parameters: $\lambda \simeq 3$ nm and $\eta = 0.5$. The partial disagreement between the model and the MC results for the case with $E_{b0} = 0$ eV in Fig. 8 is consistent with the difference between f_{1,Γ_1} and the shifted and attenuated version of f_{Γ_1} for case B in Fig. 6 at low energies. For larger E_{b0} the error in Fig. 8 is lower, again consistently with the matching between f_{1,Γ_1} and the shifted/attenuated version of f_{Γ_1} in Fig. 6 for case B above ≈ 1 eV.

E. IMPACT OF THE BAND STRUCTURE OF THE PASSIVATION LAYER

So far, we have assumed the same electron dispersion relationship in the passivation layer and in the AlGaN.

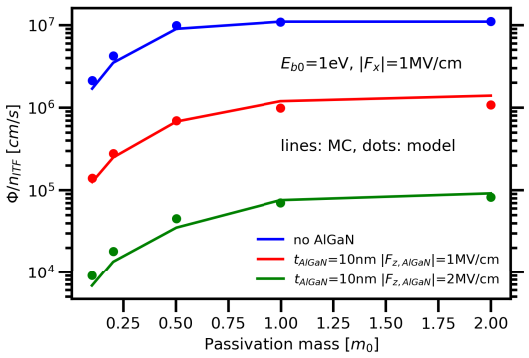

FIGURE 10. **Flux into the passivation normalized to the interface concentration in the GaN, for structures with and without AlGaN layer, as a function of the effective mass in the passivation. Dots: MC simulations, solid lines: analytical model.**

To validate the correctness of Eq. (8), Fig. 10 compares the analytical model to MC simulations as a function of the effective mass m_{pass} in the passivation layer. The non-parabolicity coefficient α_{pass} is set to zero for simplicity. As may be seen, Eq. (8) reproduces well the MC simulation results. The saturation at large fields can be easily interpreted using Eq. (9): for small m_{pass}, the injected flux scales almost linearly with m_{pass} itself; for large values of m_{pass}, instead, the current saturates to a limit set by the effective mass in AlGaN. We have verified that this flux is the same as the one computed by imposing only energy conservation at the AlGaN/passivation interface, without enforcing the conservation of the parallel momentum component.

F. CORRECTION TO THE INTERFACE CONCENTRATION

When implementing the equations above into a TCAD device simulator, one should consider that the normalized flux provided by the model must be multiplied by the interface (volumetric) concentration in order to retrieve the actual electron flux in $\mathrm{cm^{-2}s^{-1}}$. However, the interface concentration predicted by TCAD is, in general, different from the MC one for the same field configuration. This is due to the different transport equations (drift-diffusion, hydrodynamic), carrier statistics (Boltzmann vs Fermi), quantum corrections, etc. of TCAD compared to the one of MC simulations. To compensate for the discrepancy in interface concentration between drift-diffusion and MC, a correction factor for the drift-diffusion model can be worked out as follows.

Firstly, we note that since we deal with high-energy hot-carriers moving in the drift region, where the electron concentration is small, and numerous states are available, Pauli exclusion is not affecting the occupation functions. Furthermore, since the z-component of the current is negligible in the case of drift-diffusion transport, it is reasonable to assume a Boltzmann-like z-dependence of the occupation function. Considering Maxwellian occupation functions with an effective temperature T_{eff}, and the constant vertical field $F_{z,GaN}$, integration of $n(z)$ in the vertical direction leads to

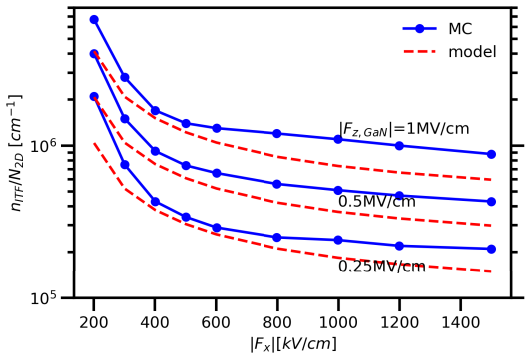

FIGURE 11. Interface volume concentration in the GaN normalized to the sheet carrier density as a function of the lateral field, for a vertical field in the GaN of 0.5 MV/cm. (blue dotted line) MC simulations, (red dashed line) analytical model.

express the interface concentration, n_{ITF}, as

$$n_{ITF} = N_{2D}\frac{q|F_{z,GaN}|}{k_B T_{eff}}, \tag{12}$$

where N_{2D} is the concentration per unit area. In the drift-diffusion and thermal-drift-diffusion models, the effective temperature T_{eff} is equal to the lattice temperature T_L. Since the MC model showed that the distributions are piece-wise Maxwellians, we define the effective temperature for the correction factor as

$$T_{eff} = \frac{T_{\Gamma_1(low)} n_{\Gamma_1(low)} + T_{\Gamma_1(high)} n_{\Gamma_1(high)} + T_U n_U}{n_{ITF}}, \tag{13}$$

where $n_{\Gamma_1(low)}$, $n_{\Gamma_1(high)}$, n_U, and n_{ITF} are given by (10) and (11). Equation (13) has been derived assuming that the vertical field in GaN is constant, and exploiting the fact that the electron distribution in GaN is a combination of heated Maxwellians. Using T_{eff} from (13), (12) matches fairly well the MC results, as shown by the dashed red line in Fig. 11. The matching can be further improved by inserting an empirical multiplication factor 1.5 (not shown). We can thus use the ratio T_L/T_{eff}, with T_{eff} given by (13), as a correction factor for the interface concentration given by the drift-diffusion simulation.

IV. DISCUSSION AND CONCLUSION

The results in Fig. 8 - 11 cover a wide range of realistic physical conditions for advanced GaN HEMT devices and deserve a more careful attention. If we consider, for instance, a device with a 10 nm AlGaN layer and a passivation layer forming a 1 eV barrier on top, we see that the ratio Φ/n_{ITF} is $\approx 10^5$ cm/s for lateral fields approaching 1 MV/cm, Fig. 8, while the interface concentration is $\approx 10^6\,\mathrm{cm}^{-1} \cdot N_{2D}$ [cm^{-2}] Fig. 11. The flux of hot-electrons above 1 eV impinging the passivation layer is thus in the order of $\Phi \approx N_{2D}[\mathrm{cm}^{-2}] \cdot 10^{11}$ [s^{-1}]. On the other hand, the flux of channel electrons per unit width drifting in the lateral direction is $\approx N_{2D}[\mathrm{cm}^{-2}] \cdot 10^7$ [cm/s], assuming an average velocity $\approx 10^7$ cm/s. Therefore, the two fluxes have comparable orders of magnitude over a length of 1 μm, meaning that, at first order, in these illustrative conditions, every electron in the channel has a chance to reach the interface between AlGaN and passivation with energy high enough for thermionic emission. Thus, the model and the MC results suggest that the passivation layer is subject to an intense bombardment of hot-carriers. This is in contrast to typical silicon MOSFET conditions, where the large Si-SiO_2 barrier makes the number of hot-carriers surmounting the barrier orders of magnitude smaller than that of the carriers in the inversion layer.

This does not *per-sé* mean that HC degradation will be fast, since the net charge and the damage generated by the hot-carriers depend on the trapping/detrapping rates at the AlGaN/passivation interface and inside the passivation layer [11], and the electric field in the passivation may be repulsive for electrons, backscattering them into the AlGaN layer before they get trapped.

Notwithstanding, the model highlights the importance of electron heating in the AlGaN layer, where the lateral electric field and backscattering in the AlGaN cannot be neglected and effectively modulate the barrier for injection in the passivation.

The proposed model can be easily integrated into commercial TCAD tools using e.g. the Physical Model Interface of Sentaurus Device [24] to calculate hot-electron injection into the passivation relevant for reliability studies.

A possible flowchart of the implementation is as follows: the injected flux can be computed as the product between Φ/n_{ITF} (given by (8) and (10)), the interface concentration given by the drift diffusion model, and the ratio T_L/T_{eff}, with T_{eff} given by (13). These quantities are computed slice by slice along the x-axis based on the local value of the lateral electric field, which provides the electron temperature through (1)-(2).

We stress that the model, in its present form, is a suitable correction for drift-diffusion simulations. Since in those simulations all carriers are assumed to be *cold*, they will typically remain in the GaN channel. Our model can be used to find the flux in the passivation without the need to solve for transport in the AlGaN barrier, as done with Fiegna's model in the simulation of hot-carrier injection in silicon MOSFETs and non-volatile memories. In hydrodynamic simulations, instead, electrons would move from GaN to AlGaN, and then from AlGaN to passivation, via thermionic emission. However, the drift-diffusion approach is numerically more robust, and requires fewer calibration parameters compared to the hydrodynamic one. Since the model compensates for discrepancies between the electron charge density in the MC transport and conventional drift-diffusion models, a consistent and accurate calculation can still be obtained.

Although being, at present, a *local* model (since hot-carrier injection at a given position is expressed in terms of the local electric field at the same position), a *non-local* version can be easily worked out by replacing the lateral field with a suitable *effective field* [17], [30].

REFERENCES

[1] M. Meneghini et al., "GaN-based power devices: Physics, reliability, and perspectives," *J. Appl. Phys.*, vol. 130, no. 18, Nov. 2021, Art. no. 181101, doi: 10.1063/5.0061354.

[2] T. McDonald, "Power conversion semiconductor and circuit trends and challenges for a sustainable energy future," in *IEDM Tech. Dig.*, Dec. 2023, pp. 1–4.

[3] F. Yang, S. Dalcanale, M. Gajda, S. Karboyan, M. J. Uren, and M. Kuball, "The impact of hot electrons and self-heating during hard-switching in AlGaN/GaN HEMTs," *IEEE Trans. Electron Devices*, vol. 67, no. 3, pp. 869–874, Mar. 2020.

[4] D. Favero et al., "R_{ON} and V_{TH} extraction in hard-switched E-mode GaN HEMTs: Impact of passivation and layout," in *Proc. IEEE Int. Rel. Phys. Symp. (IRPS)*, Apr. 2024, pp. 1–4.

[5] N. Modolo et al., "Trap-state mapping to model GaN transistors dynamic performance," *Sci. Rep.*, vol. 12, no. 1, p. 1755, Feb. 2022.

[6] A. Minetto et al., "Hot electron effects in AlGaN/GaN HEMTs during hard-switching events," *Microelectron. Rel.*, vol. 126, Nov. 2021, Art. no. 114208. [Online]. Available: https://www.sciencedirect.com/science/article/pii/S0026271421001748

[7] A. Brannick, N. Zakhleniuk, B. Ridley, L. Eastman, J. Shealy, and W. Schaff, *Modelling of Hot Electron Effects in GaN/AlGaN HEMT With AlN Interlayer*. Cham, Switzerland: Springer, 2007.

[8] A. Nakajima, S. Yagi, M. Shimizu, K. Adachi, and H. Okumura, "Hot electron induced current collapse in AlGaN/GaN HEMTs," in *Materials Science Forum*. Switzerland: Trans Tech Publications Ltd, 2007, pp. 1035–1038.

[9] L. Balestra, F. Ercolano, E. Gnani, and S. Reggiani, "TCAD modeling of high-field electron transport in bulk Wurtzite GaN: The full-band SHE-BTE," *IEEE Access*, vol. 11, pp. 6293–6298, 2023.

[10] S. Yang, S. Han, K. Sheng, and K. J. Chen, "Dynamic on-resistance in GaN power devices: Mechanisms, characterizations, and modeling," *IEEE J. Emerg. Sel. Topics Power Electron.*, vol. 7, no. 3, pp. 1425–1439, Sep. 2019.

[11] A. Minetto et al., "Drain field plate impact on the hard-switching performance of AlGaN/GaN HEMTs," *IEEE Trans. Electron Devices*, vol. 68, no. 10, pp. 5003–5008, Oct. 2021.

[12] N. Zagni, G. Verzellesi, A. Bertacchini, M. Borgarino, F. Iucolano, and A. Chini, "Hole virtual gate model explaining surface-related dynamic RON in p-GaN power HEMTs," *IEEE Electron Device Lett.*, vol. 45, no. 5, pp. 801–804, May 2024.

[13] A. Brannick, N. A. Zakhleniuk, B. K. Ridley, L. F. Eastman, J. R. Shealy, and W. J. Schaff, "Hydrodynamic simulation of surface traps in the AlGaN/GaN HEMT," *Microelectron. J.*, vol. 40, no. 3, pp. 410–412, Mar. 2009.

[14] T. Grasser, T.-W. Tang, H. Kosina, and S. Selberherr, "A review of hydrodynamic and energy-transport models for semiconductor device simulation," *Proc. IEEE*, vol. 91, no. 2, pp. 251–274, Feb. 2003.

[15] C. Hu, "Lucky-electron model of channel hot electron emission," in *IEDM Tech. Dig.*, 1979, pp. 22–25.

[16] K. Hasnat et al., "A pseudo-lucky electron model for simulation of electron gate current in submicron NMOSFET's," *IEEE Trans. Electron Devices*, vol. 43, no. 8, pp. 1264–1273, Aug. 1996.

[17] C. Fiegna, F. Venturi, M. Melanotte, E. Sangiorgi, and B. Ricco, "Simple and efficient modeling of EPROM writing," *IEEE Trans. Electron Devices*, vol. 38, no. 3, pp. 603–610, Mar. 1991.

[18] L. Selmi et al., "Verification of electron distributions in silicon by means of hot carrier luminescence measurements," *IEEE Trans. Electron Devices*, vol. 45, no. 4, pp. 802–808, Apr. 1998.

[19] U. V. Bhapkar and M. S. Shur, "Monte Carlo calculation of velocity-field characteristics of Wurtzite GaN," *J. Appl. Phys.*, vol. 82, no. 4, pp. 1649–1655, Aug. 1997, doi: 10.1063/1.365963.

[20] J. D. Albrecht, R. P. Wang, P. P. Ruden, M. Farahmand, and K. F. Brennan, "Electron transport characteristics of GaN for high temperature device modeling," *J. Appl. Phys.*, vol. 83, no. 9, pp. 4777–4781, May 1998, doi: 10.1063/1.367269.

[21] S. Yamakawa, R. Akis, N. Faralli, M. Saraniti, and S. M. Goodnick, "Rigid ion model of high field transport in GaN," *J. Phys., Condens. Matter*, vol. 21, no. 17, Apr. 2009, Art. no. 174206, doi: 10.1088/0953-8984/21/17/174206.

[22] J. Fang, M. V. Fischetti, R. D. Schrimpf, R. A. Reed, E. Bellotti, and S. T. Pantelides, "Electron transport properties of $Al_xGa_{1-x}N$/GaN transistors based on first-principles calculations and Boltzmann- equation Monte Carlo simulations," *Phys. Rev. Appl.*, vol. 11, Apr. 2019, Art. no. 044045. [Online]. Available: https://link.aps.org/doi/10.1103/PhysRevApplied.11.044045

[23] S. Wang et al., "Comparison the electron momentum and energy relaxation process in Wurtzite GaN, InN and AlN by Monte Carlo method," *Solid State Commun.*, vol. 288, pp. 68–73, Feb. 2019. [Online]. Available: https://www.sciencedirect.com/science/article/pii/S0038109818309074

[24] *Sentaurus Device User Guide, Synop.*, USA, 2024.

[25] P. Palestri, L. Sayadi, A. Minetto, G. Prechtl, L. Selmi, and O. Häberlen, "Monte Carlo analysis of hot electron injection in the passivation layer of GaN HEMTs," *Solid-State Electron.*, vol. 230, Dec. 2025, Art. no. 109257. [Online]. Available: https://www.sciencedirect.com/science/article/pii/S0038110125002023

[26] A. Dyson, D. R. Naylor, and B. K. Ridley, "Hot-phonon effects on high-field transport in GaN and AlN," *IEEE Trans. Electron Devices*, vol. 62, no. 11, pp. 3613–3618, Nov. 2015.

[27] S. Vitanov, M. Nedjalkov, and V. Palankovski, "*A Monte Carlo model of piezoelectric scattering in GaN*," in *Numerical Methods and Applications*. Springer, 2007, pp. 197–204.

[28] R. Clerc, P. Palestri, and L. Selmi, "On the physical understanding of the kT-layer concept in quasi-ballistic regime of transport in nanoscale devices," *IEEE Trans. Electron Devices*, vol. 53, no. 7, pp. 1634–1640, Jul. 2006.

[29] S. M. Sze and K. K. Ng, *Physics of Semiconductor Devices*. Hoboken, NJ, USA: Wiley, 2007.

[30] P. Palestri, L. Selmi, G. A. M. Hurkx, J. W. Slotboom, and E. Sangiorgi, "Energy dependent electron and hole impact ionization in Si bipolar transistors," in *IEDM Tech. Dig.*, 1998, pp. 885–888.